First Passage Time Analysis on Climate Indices

Peter C. Chu
Naval Ocean Analysis and Prediction Laboratory, Naval Postgraduate School
Monterey, CA 93943

Report Documentation Page		*Form Approved* *OMB No. 0704-0188*

Public reporting burden for the collection of information is estimated to average 1 hour per response, including the time for reviewing instructions, searching existing data sources, gathering and maintaining the data needed, and completing and reviewing the collection of information. Send comments regarding this burden estimate or any other aspect of this collection of information, including suggestions for reducing this burden, to Washington Headquarters Services, Directorate for Information Operations and Reports, 1215 Jefferson Davis Highway, Suite 1204, Arlington VA 22202-4302. Respondents should be aware that notwithstanding any other provision of law, no person shall be subject to a penalty for failing to comply with a collection of information if it does not display a currently valid OMB control number.

1. REPORT DATE **2008**	2. REPORT TYPE	3. DATES COVERED **00-00-2008 to 00-00-2008**
4. TITLE AND SUBTITLE **First Passage Time Analysis on Climate Indices**		5a. CONTRACT NUMBER
		5b. GRANT NUMBER
		5c. PROGRAM ELEMENT NUMBER
6. AUTHOR(S)		5d. PROJECT NUMBER
		5e. TASK NUMBER
		5f. WORK UNIT NUMBER
7. PERFORMING ORGANIZATION NAME(S) AND ADDRESS(ES) **Naval Postgraduate School,Department of Oceanography,Monterey,CA,93943**		8. PERFORMING ORGANIZATION REPORT NUMBER
9. SPONSORING/MONITORING AGENCY NAME(S) AND ADDRESS(ES)		10. SPONSOR/MONITOR'S ACRONYM(S)
		11. SPONSOR/MONITOR'S REPORT NUMBER(S)
12. DISTRIBUTION/AVAILABILITY STATEMENT **Approved for public release; distribution unlimited**		
13. SUPPLEMENTARY NOTES		
14. ABSTRACT		
15. SUBJECT TERMS		

16. SECURITY CLASSIFICATION OF:			17. LIMITATION OF ABSTRACT	18. NUMBER OF PAGES	19a. NAME OF RESPONSIBLE PERSON
a. REPORT **unclassified**	b. ABSTRACT **unclassified**	c. THIS PAGE **unclassified**	**Same as Report (SAR)**	**30**	

Standard Form 298 (Rev. 8-98)
Prescribed by ANSI Std Z39-18

Abstract

Climate variability is simply represented by teleconnection patterns such as the Arctic Oscillation (AO), Antarctic Oscillation (AAO), North Atlantic Oscillation (NAO), Pacific/North American Pattern (PNA), and Southern Oscillation (SO) with associated indices. Two approaches can be used to predict the indices: forward and backward methods. The forward method is commonly used to predict the index fluctuation ρ at time t with a given temporal increment τ. Using this method, it was found that the index (such as for NAO) has the Brownian fluctuations. On the base of the first passage time (FPT) concept, the backward method is introduced in this study to predict the typical time span (τ) needed to generate a fluctuation in the index of a given increment ρ. After the five monthly indices (AO, AAO, NAO, PNA, SO) running through the past history, the FPT density functions are obtained. FPT presents a new way to detect the temporal variability of the climate indices. The basic features for the index prediction are also discussed.

1. Introduction

Complexity in climate systems makes the prediction difficult. One way to simplify the climate systems is to represent low-frequency variability of atmospheric circulations by teleconnection patterns, such as the Arctic Oscillation (AO), Antarctic Oscillation (AAO), North Atlantic Oscillation (NAO), Pacific/North American Pattern (PNA), and Southern Oscillation (SO). Temporally varying indices, $s(t)$, were calculated for these patterns. Here, t denotes time.

Among them, the SO index (SOI) was first to use showing equivalent barotropic seasaw in atmospheric pressure between the southeastern tropical Pacific and the Australian-Indonesian regions (Walker and Bliss 1937). A popular formula for calculating the monthly SOI is proposed by the Australian Bureau of Meteorology,

$$s(t) = 10 \times \frac{p_{\text{diff}}(t) - \langle p_{\text{diff}} \rangle}{SD(p_{\text{diff}})}. \tag{1}$$

Here, p_{diff} is the mean sea level pressure of Tahiti minus that of Dawin for that month; $\langle p_{\text{diff}} \rangle$ is the long term average of p_{diff} for the month in question; and $SD(p_{\text{diff}})$ is the long term standard deviation of p_{diff} for the month in question. The SOI ranges from about -35 to about $+35$.

The indices of the other oscillations (AO, AAO, NAO, PNA) are the expansions of similar seasaw phenomenon such as the Northern Hemisphere annular mode [or called AO] and the two patterns (i.e., NAO and AO) as "two-paradigms of the same phenomenon" (Wallace 2000). These oscillation patterns are usually calculated on the base of the Rotated Principal Component Analysis (RPCA) (Barnston and Livezey 1987). Monthly (AO, AAO, NAO, PNA) indices are constructed by projecting the monthly

mean (1000-, 700-, 500-, 500-hPa) height anomalies onto the leading EOF mode. The time series are normalized by the standard deviation of the monthly index. Since the loading pattern of (AO, AAO, NAO, PNA) is obtained using the monthly mean height anomaly dataset, the index corresponding to each loading pattern becomes one when it is normalized by the standard deviation of the monthly index. Detailed information is referred to the website: http://www.cpc.noaa.gov/.

Long-term time series of the climate indices represent invaluable sources of information to represent the complex seasonal, interannual, and interdecadal variabilities of the climate systems. For example, sustained negative values of the SOI often indicate El Nino episodes. These negative values are usually accompanied by sustained warming of the central and eastern tropical Pacific Ocean, a decrease in the strength of the Pacific trade winds, and a reduction in rainfall over eastern and northern Australia. Positive values of the SOI are associated with stronger Pacific trade wind and warmer sea temperatures to the north of Australia, popularly known as a La Nina episode. Waters in the central and eastern tropical Pacific Ocean become cooler during this time. Together these give an increased probability that eastern and northern Australia will be wetter than normal. The SOI has been used in numerous studies as an indicator of the status of the ENSO phenomenon and as a predictor for global and regional climatic prediction such as temperature (e.g., Smith and Sterns, 1993), precipitation (e.g., Ropelewski and Halpert, 1987), and agricultural products (e.g., Rimmington and Nicholls, 1993). The other indices have similar features.

How to predict effectively the climate indices has practical significance due to their connections to the large scale atmospheric circulations. Usually, these indices are

treated as time series and statistical predictions are conducted (forward method). For example, the singular spectrum analysis (Keppenne and Ghil 1992), the wavelet analysis (Torrence and Campo 1998), and the nonlinear analog analysis (Drosdowsky 1994) were used to obtain the dominant frequencies of the SOI time series. The power-law correlations were found for the self-affine properties of SOI (Ausloos and Ivanova 2001).

It may possible use an alternative "backward" method, which predicts a typical time span (τ) needed to generate a fluctuation in the index of a given increment ρ. This method is established on the base of the first passage time (FPT) concept, which is widely used in many disciplines such as physics, chemistry, biology, and economics, etc., but not in meteorology until recently when Chu et al. (2002a, b) used FPT to study the ocean-atmospheric model predictability. The major purpose of this paper is to show the usefulness of FTP on the climate index prediction.

The rest of the paper is outlined as follows. Section 2 discusses the two approaches to predict the climate indices. Section 3 shows the FPT concept, applied in this paper. Section 4 investigates the sensitivity of the FPT density function to the index reduction ρ. Section 5 shows the power-law dependence of optimal FPT on the index reduction density ρ and classifies the variability of the climate indices as the Brownian motion using the FPT. Finally, Section 6 presents the conclusions.

2. Forward and Backward Approaches of Prediction

Monthly varying climate indices from the NOAA Climate Prediction Center show randomness (Figure 1) with poor predictability because their phases and amplitudes are rather unpredictable with both involving many (time and space) scales which are often intrinsic to chaotic behavior; see reviews for the NAO index (Palmer 2000; Greatbatch

5

2000; Wanner et al. 2001). The histograms of the monthly mean indices show Gaussian-type distributions with mean values near-zero for all the indices (AO: -0.136, AAO: -0.01, NAO: -0.004, PNA: 0.018, SOI: -0.077) and with standard deviations near 1 for AO (0.981), AAO (0.989), NAO (0.985), and near 10 for SOI (10.5) (Figure 2).

Both forward and backward approaches exist in index prediction. The forward approach predicts the change of the index (ρ) at time t with a given temporal increment τ from analyzing single or multiple time series. Due to stochastic nature, the probability density function (PDF), $p[\rho(t),\tau]$, should be first constructed. Collette and Ausloos (2004) analyzed the NAO monthly index (single time series) from 1825 till 2002 and found that the long range time correlations are similar to Brownian fluctuations. The distribution functions of the NAO monthly index fluctuations have a form close to a Gaussian, for all time lags. This indicates the lack of predictive power of the present NAO monthly index. Lind et al. (2005) used the standard Markov analysis to get the Chapman-Kolmogorov equation for the conditional PDF of the increments ρ of the NAO index over different time intervals τ and to compute the diffusion and drift coefficients ($D^{(1)}$, $D^{(2)}$) from the first two moments of such probability distribution. The random variable $\rho(t)$ is found to satisfy the Langevin equation

$$\frac{d\rho(t)}{dt} = D^{(1)}\left[\rho(t),t\right] + \eta(t)\sqrt{D^{(2)}\left[\rho(t),t\right]} \tag{2}$$

where $\eta(t)$ is a fluctuating δ-correlated force with Gaussian statistics, i.e.,

$$\langle\eta(t)\eta(t')\rangle = 2\delta(t-t').$$

Maharaj and Wheeler (2005) predict the daily bi-variate index (multiple time series) of the Madden-Julian oscillation using seasonally varying vector autoregressive (VAR)

models. The first-order VAR model on the original (non-differenced) time series was found to be the most satisfactory for forecasting the index beyond a few days. Although this model shows no strong skill advantage over a lagged regression technique, it has the convenience of employing only a single set of equations to make predictions for multiple forecast horizons.

The backward approach predicts the typical time span (τ) needed to generate a fluctuation in the index of a given increment ρ. To do so, the FPT concept is used. As the index date runs through the past history, the accumulated values of the FPTs form the PDF (called FPT density function). The mode of the PDF shows the most probable time when the index decreases with the value of ρ at the first time.

The FPT is important from a prediction point of view in several ways. First, although the climate indices are related to certain circulation patterns such as the negative SOI values generally connecting to the El Nino events, one still does not know the exact time of the El Nino onset. Therefore, the best one can do, from a statistical point of view, is to make a prediction at a time that is probabilistically favorable. This optimal time, as we will see, is determined by the maximum of the FPT density function, i.e. the optimal FPT. Second, but not least, the FPT density function will by itself give invaluable, non-trivial information about the stochasticity of the climate indices. Third, FPT effectively represents the ocean-atmospheric model predictability (Chu et al., 2002a, b).

3. FPT

In a series papers, Chu et al. (2002a) introduced the FPT (τ) concept into the ocean-atmospheric model predictability with the model error (i.e., 'some quantity') first exceeding a predetermined tolerance level (i.e., 'predetermined criterion'), found the FPT

7

density function satisfying the backward Fokker-Planck equation, and obtained the analytical solution of the FPT density function for the nonlinear simplified low-order Lorenz atmospheric model (Nicolis 1992). Both linear and nonlinear perspectives of forecast errors are analytically investigated (Chu et al. 2002b). Furthermore, the FPT was also used to evaluate the full physical nowcast/forecast ocean prediction system. For example, the FPT density function is asymmetric with a broader and long tail in higher value side, which indicates long-term predictability. The long-term (extreme long) predictability is not an "outlier" and shares the same statistical properties as the short-term predictions (Chu et al. 2002c). The FPT is also used to verify the model ability to predict Lagrangian drifter trajectories (Chu et al. 2004) and the regional ocean model predictability to stochastic perturbations in initial conditions, winds, and open boundary conditions (Chu et al. 2005).

Using the same concept, the FPT is used to explore the statistical features of the time series of climate indices. They change either positively or negatively at a given time (Figure 1). Then, of course, it is interested in predicting the exact change at a point in time. However, it is not possible. Therefore, the best one can do, from a statistical point of view, is to predict the time that is probabilistically favorable for the given index change. This optimal time, as we will see, is determined by the maximum of the first passage time distribution, i.e. the optimal FPT.

Given a fixed value of an index reduction (ρ), the corresponding time span (positive) is estimated for which the index reduction

$$\gamma_{\Delta t}(t) = s(t + \Delta t) - s(t), \qquad (3)$$

reaches the level ρ for the first time,

8

$$\tau_\rho(t) = \inf\left\{\Delta t > 0 \,|\, \gamma_{\Delta t}(t) \leq -\rho\right\}, \qquad (4)$$

which is called the FPT. It is noted that similar definition can be used for the index enhancement. As the index data run through the past history which is represented by (2), the FPT density function satisfies the backward Fokker-Planck equation (Chu et al. 2002a)

$$\frac{\partial p}{\partial t} - \left[D^{(1)}(\rho,t)\right]\frac{\partial p}{\partial \rho} - \frac{1}{2}\eta^{(2)}D^{(2)}(\rho,t)\frac{\partial^2 p}{\partial \rho^2} = 0. \qquad (5)$$

The cumulative distribution is introduced for the transition time being larger than τ_ρ, i.e.

$$P(\tau_\rho) = \int_{\tau_\rho}^{\infty} p(\tau)d\tau. \qquad (6)$$

All the five climate indices show similar Gaussian-type distributions (Figure 2). The Brownian fluctuations identified in NAO monthly index (Collette and Ausloos 2004) may extend to the other indices. For the Brownian fluctuations with zero drift, the FPT density function has the analytical solution for finite ρ (Rangarajan and Ding 2000),

$$p(\tau) = \frac{1}{\sqrt{\pi}}\frac{a}{\tau^{3/2}}\exp\left(-\frac{a^2}{\tau}\right), \quad a > 0, \quad \tau > 0. \qquad (7)$$

Here, a is a function of ρ. With $\rho \to 0$ as a limit case (i.e., no index reduction), the FPT tends to 0 with a probability of 100%. Thus, the FPT density function cannot be represented by (7) but the δ function,

$$p(\tau) \to \delta(\tau), \quad \text{as} \quad \rho \to 0.$$

The maximum value of $p(\tau)$ (for finite ρ) indicates the most favorable FPT,

$$\tau_\rho^{(\max)} = \frac{2a^2}{3}. \qquad (8)$$

With the known FPT density function (7), the k-th moment ($k = 1, 2, \ldots$) of FPT for

finite ρ is calculated by

$$M_k(\rho) = k\int_0^\infty p(\tau)\tau^{k-1}d\tau, \qquad k = 1, \ldots, \infty. \tag{9}$$

The mean and variance of FPT can be calculated from the first two moments

$$\langle \tau_\rho \rangle = M_1, \tag{10}$$

$$\langle \delta\tau_\rho^2 \rangle = M_2 - M_1^2, \tag{11}$$

where the bracket denotes the average over realizations.

4. Sensitivity of $p(\tau_\rho)$ with Respect to ρ

The theoretical distribution (7) solely depends on the parameter a. This parameter

can be determined from the monthly index data. First, the FPT density functions are

constructed and fitted to (7) for each index with various values of index reduction ρ.

For example, Figure 3 shows $p(\tau_\rho)$ with $\rho = 1.9$ for (AO, AAO, NAO, PNA) indices

and with $\rho = 25$ for SOI. Note that almost an order of difference in ρ-values (1.9 versus

25) is selected. This is due to the different ranges of index fluctuation: (-4, 4) for (AO,

AAO, NAO, PNA) indices and (-40, 40) for SOI. It exhibits a rather well defined and

pronounced maximum, followed by an extended tail for very long FPTs indicating a non-

zero and important probability of large passage times (note that the τ_ρ-axis is

logarithmic). These long (toward El Nino for SOI) FPTs reflect periods where the

tropical Pacific is in a strong El Nino phase and needs a long period of time before

finally coming to an even stronger El Nino. The short FPTs on the other hand – those

around the maximum – are in La Nina periods, which appear to be the most common scenario.

Second, for each index reduction (ρ), the parameter (a) is determined from the τ_ρ data fitted to (7). From the scatter diagram for each index (Figure 4), the linear relationship between (a, ρ),

$$a = \alpha_1 + \alpha_2 \rho, \tag{12}$$

is found using the least square method. Here, Eq.(12) represents the (NAO, NPA, SOI) indices quite well, but not too well for the (AO, AAO) indices since oscillations around the linear trend are found. Despite oscillations, the linear correlation between a and ρ is very evident with positive regression coefficient α_2 (Table 1).

To better understand the tail of this distribution, various values of ρ are considered. If this level is small enough, it is likely that the index reduction will break through the level after the first month, while larger FPTs will become more and more unlikely. However, the probability for a large FPT value will not be zero; if, say, a small level ρ, then a period of strong El Nino will result in a $\tau_\rho(t)$ that might be considerably larger than one month since it takes time to recover from the El Nino event. For instance, after the 1992 El Nino event, it took five years to reach a new El Nino event in 1997.

5. Characteristics of the Index Variability – Brownian Motion

A random process is called fractional Brownian motion if its cumulative FPT density function satisfies the power law (Ding and Yang 1995),

$$P(\tau) \sim \tau^{H-1}, \tag{13}$$

11

with $0 < H < 1$. Here H is the Hurst exponent. For $H = 1/2$, the random process is the ordinary Brownian motion. The cumulative distribution, $P(\tau_\rho)$, for each climate index data (Figure 5) shows a power law feature in the tail of the distribution scales. For a very small value of the index reduction, ρ_0 (0.01 for the AO, AAO, NAO, and PNA indices and 0.1 for SOI), the cumulative FPT density function calculated from the index data shows that

$$P(\tau_0) \sim \tau_0^{-\alpha_0}, \tag{14}$$

with $\alpha_0 \sim 1/2$. Since the Hurst exponent of an ordinary Brownian motion is $H = 1/2$, the empirically observed scaling (see Figure 5) is a consequence of the (at least close to) Brownian motion behavior of the climate indices. This argument of an unbiased Brownian motion is also strengthen by observing that (see Figure 5)

$$P(\tau_0 = 1) \sim 1/2. \tag{15}$$

This indicates that the climate index has 50% chance of increase and decrease at each time step (one month).

Figure 5 also shows the cumulative distributions $P(\tau_\rho)$ for different values of ρ, i.e., $\rho = 0.5, 1.0,$ and 1.5 for the (AO, AAO, NAO, PNA) indices and $\rho = 10, 20,$ and 30 for SOI. From this figure it is seen that the tail exponent, α_ρ, is rather insensitive to the value of ρ. In particular one finds that $\alpha_\rho \sim 1/2$ over a broad range of values for ρ, a value that is consistent with the Brownian motion hypothesis.

Moreover, it is noted that as the level ρ is increased from zero, the optimal FPT ($\tau_\rho^{(max)}$) moves away from $\tau_0 = 1$ and toward larger values. How does the optimal FPT

$\tau_\rho^{(\max)}$ depend on the level ρ for large ρ? This dependence, as measured from the empirical distribution (i.e., the histogram of FPT), is shown in Figure 6. Intuitively, it is clear that the optimal FPT will increase as ρ increases.

The power law is found for the optimal FPT versus ρ,

$$\tau_\rho^{(\max)} \sim \rho^\gamma \quad \text{for large } \rho, \tag{16}$$

with $\gamma \sim 2.0$ for the AO, AAO, and SO indices and $\gamma \sim 1.0$ for the NAO and PNA indices (see Figure 7), which consists with the results for a Brownian motion with the theoretical FPT density function [see (7) and (8)]. Substituting (12) into (8) gives

$$\tau_\rho^{(\max)} = \alpha_2^2 \rho^2 + 2\alpha_1 \alpha_2 \rho + \alpha_1^2. \tag{17}$$

The exponent of the power-law depends on the regression coefficients (α_1, α_2) (see Table -1). Large ρ usually means much larger than 1 for the SOI, and slightly larger than 1 for the AO, AAO, NAO, and PNA indices. For the SOI, the regression coefficients are given by $\alpha_1 = 0.165$, $\alpha_2 = 0.125$, the leading term of (17) is $\alpha_2^2 \rho^2$, and therefore, the exponent of the power-law is around 2. For the AO and AAO indices, α_2 is larger than α_1. The leading term of (17) is $\alpha_2^2 \rho^2$ for large ρ, and therefore, the exponent of the power-law is around 2. However, for the NAO and PNA indices, α_2 is smaller than α_1. The leading term of (17) is $2\alpha_1 \alpha_2 \rho$ for large ρ, and therefore, the exponent of the power-law is around 1. Not surprisingly, there are some deviations from standard theories for the variation of the optimal FPT with the level ρ (i.e., the straight line). Furthermore, we have checked, and found, that there is an approximate symmetry under

$$\rho \to -\rho$$

for the FPT density function. One therefore does not have to consider index enhancement explicitly.

6. Conclusions

(1) FPT presents a new way to detect the temporal variability of the climate indices. It predicts a typical time span (τ) needed to generate an index reduction of a given increment ρ. FPT is a random variable and whose density function satisfies the backward Fokker-Planck equation. Solving this equation, it is easy to obtain the ensemble mean and variance of the FPT of the climate indices.

(2) FPTs for the five climate indices show the Brownian fluctuations. This means that the early results on the Brownian fluctuations for the NAO index (e.g., Collette and Ausloos 2004) are also valid for the other indices (AO, AAO, PNA, and SO). With $\delta \to 0$ as a limit case (i.e., no index reduction), the FPT density function tends to the δ function.

(3) For a very small value of the index reduction, ρ_0 (0.01 for the AO, AAO, NAO, and PNA indices and 0.1 for SOI), the cumulative FPT density function shows the power-law dependence on τ_ρ with the exponent approximately -1/2. Another well known method to check power-law dependence is examination of the autocorrelation function. This also confirms that the climate indices have the Brownian-type fluctuations.

(4) The optimal FPT has a power-law dependence on the index reduction (ρ) for large ρ with the exponent (~2) for the AO, AAO and SO indices and (~1) for the NAO and PNA indices.

(5) The FPT density functions as well as the variation of the optimal FPT can be applied if one wants to estimate the most probable time period needed for the low-

14

frequency atmospheric circulation pattern to sustain if a prediction aims at a specific optimal transition.

(6) The FPT analysis can be applied to other air-ocean time series.

Acknowledgment

References

Ausloos, M., and K. Ivanova, 2001: Power-law correlations in the southern-oscillation-index fluctuations characterizing El Nino. *Phys. Rev. E*, **63**, 047201.

Barnston, G., and R. E. Livezey, 1987: Classification, seasonality and low-frequency atmospheric circulation patterns. *Mon. Wea. Rev.,* **115,** 1083–1126.

Chu, P.C., L.M. Ivanov, C.W. Fan, 2002a: Backward Fokker-Planck equation for determining model valid prediction period. *J. Geophys. Res*., **107**, 10.1029/2001JC000879.

Chu, P.C., L.M., Ivanov, T.M. Margolina, and O.V. Melnichenko, 2002b: On probabilistic stability of an atmospheric model to various amplitude perturbations. *J. Atmos. Sci*., **59**, 2860-2873.

Chu, P.C., L. Ivanov, L. Kantha, O. Melnichenko, and Y. Poberezhny, 2002c: Power law decay in model predictability skill. *Geophys. Res. Lett*., **29**, 10.1029/2002GLO14891.

Chu, P.C., L.M. Ivanov, L.H. Kantha, T.M. Margolina, and O.M. Melnichenko, and Y.A, Poberenzhny, 2004: Lagrangian predictabilty of high-resolution regional ocean models. *Nonlinear Proc. Geophys*., **11**, 47-66.

Chu, P.C., and L.M. Ivanov, 2005: Statistical characteristics of irreversible predictability time in regional ocean models. *Nonlinear Proc. Geophys*., **12**, 1-10.

Collette, C., and M. Ausloos, 2004: Scaling analysis and evolution equation of the North Atlantic oscillation index fluctuations. *Int. J. Mod. Phys*. *C*, **15**, 1353-1366.

Ding, M., and W. Yang, 1995: Distribution of the first return time in fractional Brownian motion and its application to the study of on-off intermittency. *Phys. Rev. E*, **52**, 207-213.

Drosdowsky, W, 1994: Analog (nonlinear) forecasts of the Southern Oscillation index time series. *Wea. Forcast*., **9**, 78-84.

Greatbatch, R. J., 2000: The North Atlantic Oscillation. *Stochastic Environ. Res. Risk Assess*, **14**, 213-242.

Keppenne, C. L., and M. Ghil, 1992: Adaptive spectral analysis and prediction of the Southern Oscillation index. *J. Geophys. Res.,* **97,** 20449–20454.

Lind, P. G., A. Mora, J. A. C. Gallas, and M. Haase, 2005: Reducing stochasticity in the North Atlantic Oscillation index with coupled Langevin equations. *Phys. Rev. E*, **72**, 056706.

Maharaj, E. A., and M. J. Wheeler, 2005: Forecasting an index of the Madden-Julian Oscillation. *Int. J. Climatol*., **25**, 1611-1618.

Nicolis, C., 1992: Probabilistic aspects of error growth in atmospheric dynamics. *Quart. J. Roy. Meteor. Soc*., **118**, 553-568.

Palmer, T.N., 2000: Predicting uncertainty in forecasts of weather and climate. *Rep. Prog. Phys*., **63**, 71-116.

Rangarajan, G. and M. Ding, M, 2000: First passage time distribution for anomalous diffusion. *Phys. Lett. A*, **273**, 322-330.

Rimmington, G. M., and N. Nicholls, 1993: Forecasting wheat yields in Australia with the Southern Oscillation index. *Austral. J. Agricul. Res*., **44**, 625 – 632.

Ropelewski, C. F., and M.S. Halpert, 1987: Global and regional scale precipitation patterns associated with the El Nino/Southern Oscillation. *Mon. Wea. Rev*., **115**, 1606-1626.

Smith, S.R., and C. R. Sterns, 1993: Antarctic pressure and temperature anomalies surrounding the minimum in the Southern Oscillation index. *J. Geophys. Res*., **98**, 13071–14752.

Torrence, C., and G. P. Campo, 1998: A practical guide to wavelet analysis. *Bull. Amer. Meteor. Soc.*, **79**, 62-78.

Walker, G. T., and E. W. Bliss, 1937: World weather VI. *Mem. Roy. Meteor. Soc.,* **4,** 119–139.

Wallace, J.M., 2000: North Atlantic Oscillation/annular mode: two paradigms? one phenomenon. *Quart. J. Royal Met. Soc*., **126**, 791-805.

Wanner, H., S. Bronnimann, C. Casty, D. Gyalistras, J. Luterbacher, C. Schmutz, D.B. Stephenson, and E. Xoplaki, 2001: North Atlantic Oscillation - concepts and studies. *Surv. Geophys*., **22**, 321-382.

Table Captions

Table 1. Coefficients (α_1, α_2) in Eq.(12) for the five climate indices.
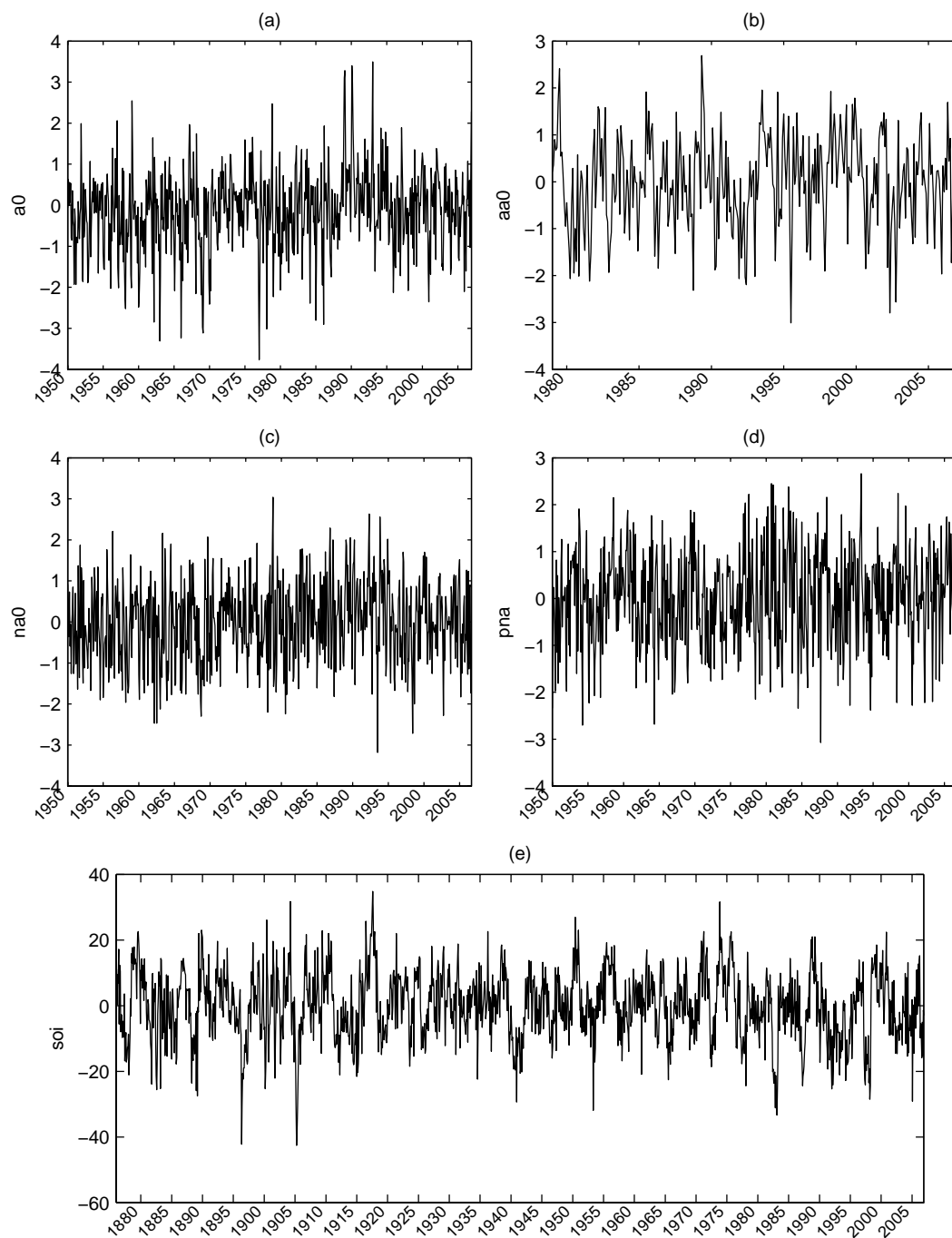
Figure Captions

Figure 1.   The monthly mean climate index data obtained from NOAA Climate Prediction Center for: (a) Arctic Oscillation (AO), (b) Antarctic Oscillation (AAO), (c) North Atlantic Oscillation (NAO), (d) Pacific/North American Pattern (PNA), and (e) Southern Oscillation (SO). Detailed information is referred to the website: http://www.cpc.noaa.gov/.

Figure 2. Histograms of the climate indices: (a) Arctic Oscillation (AO), (b) Antarctic Oscillation (AAO), (c) North Atlantic Oscillation (NAO), (d) Pacific/North American Pattern (PNA), and (e) Southern Oscillation (SO).

Figure 3. FPT density functions with particular index reduction ρ for (a) Arctic Oscillation (AO), (b) Antarctic Oscillation (AAO), (c) North Atlantic Oscillation (NAO), (d) Pacific/North American Pattern (PNA), and (e) Southern Oscillation (SO).

Figure 4. Linear relation ship between the parameter a in the FPT density function and the index reduction δ for (a) Arctic Oscillation (AO), (b) Antarctic Oscillation (AAO), (c) North Atlantic Oscillation (NAO), (d) Pacific/North American Pattern (PNA), and (e) Southern Oscillation (SO).

Figure 5. The empirical cumulative density functions, $P(\tau_\rho)$, for different values of the index reduction ρ for (a) Arctic Oscillation (AO), (b) Antarctic Oscillation (AAO), (c)

21

North Atlantic Oscillation (NAO), (d) Pacific/North American Pattern (PNA), and (e) Southern Oscillation (SO). It shows the power-law features.

Figure 6. FPT density function of SOI with different values of ρ : (a) 15, (b) 20, (c) 25, and (d) 30. It is noted that the optimal FPT increases as ρ increases.

Figure 7. Dependence of the optimal FPT, $\tau_\rho^{(\mathrm{max})}$, on the index reduction ρ for (a) Arctic Oscillation (AO), (b) Antarctic Oscillation (AAO), (c) North Atlantic Oscillation (NAO), (d) Pacific/North American Pattern (PNA), and (e) Southern Oscillation (SO). Power-law exists for large ρ values.

Table 1. Coefficients (α_1, α_2) in Eq.(12) for the five climate indices.

	AO	AAO	NAO	PNA	SO
α_1	0.430	0.508	0.604	0.600	0.165
α_2	0.696	0.562	0.351	0.373	0.125

Figure 1. The monthly mean climate index data obtained from NOAA Climate Prediction Center for: (a) Arctic Oscillation (AO), (b) Antarctic Oscillation (AAO), (c) North Atlantic Oscillation (NAO), (d) Pacific/North 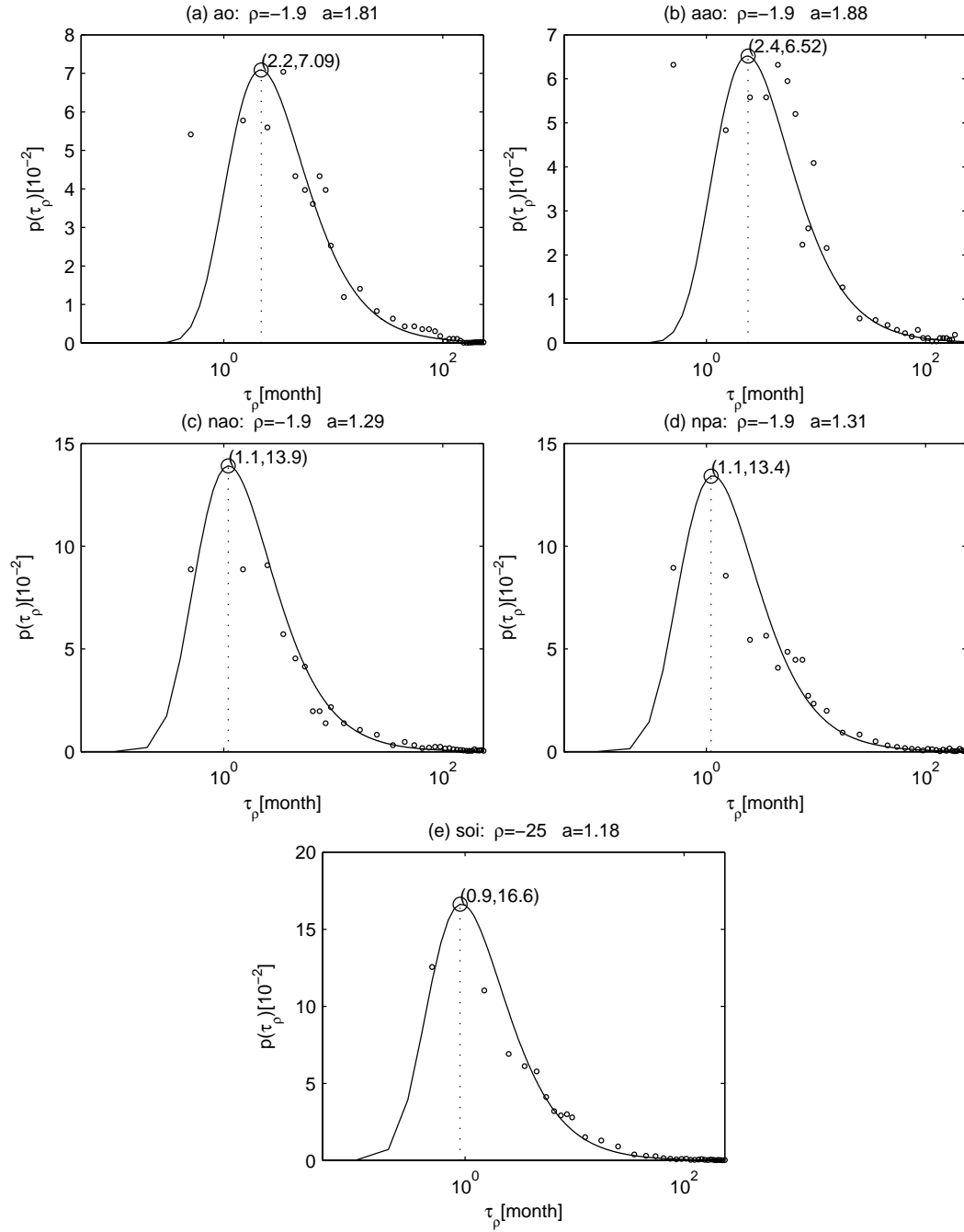American Pattern (PNA), and (e) Southern Oscillation (SO). Detailed information is referred to the website: http://www.cpc.noaa.gov/.
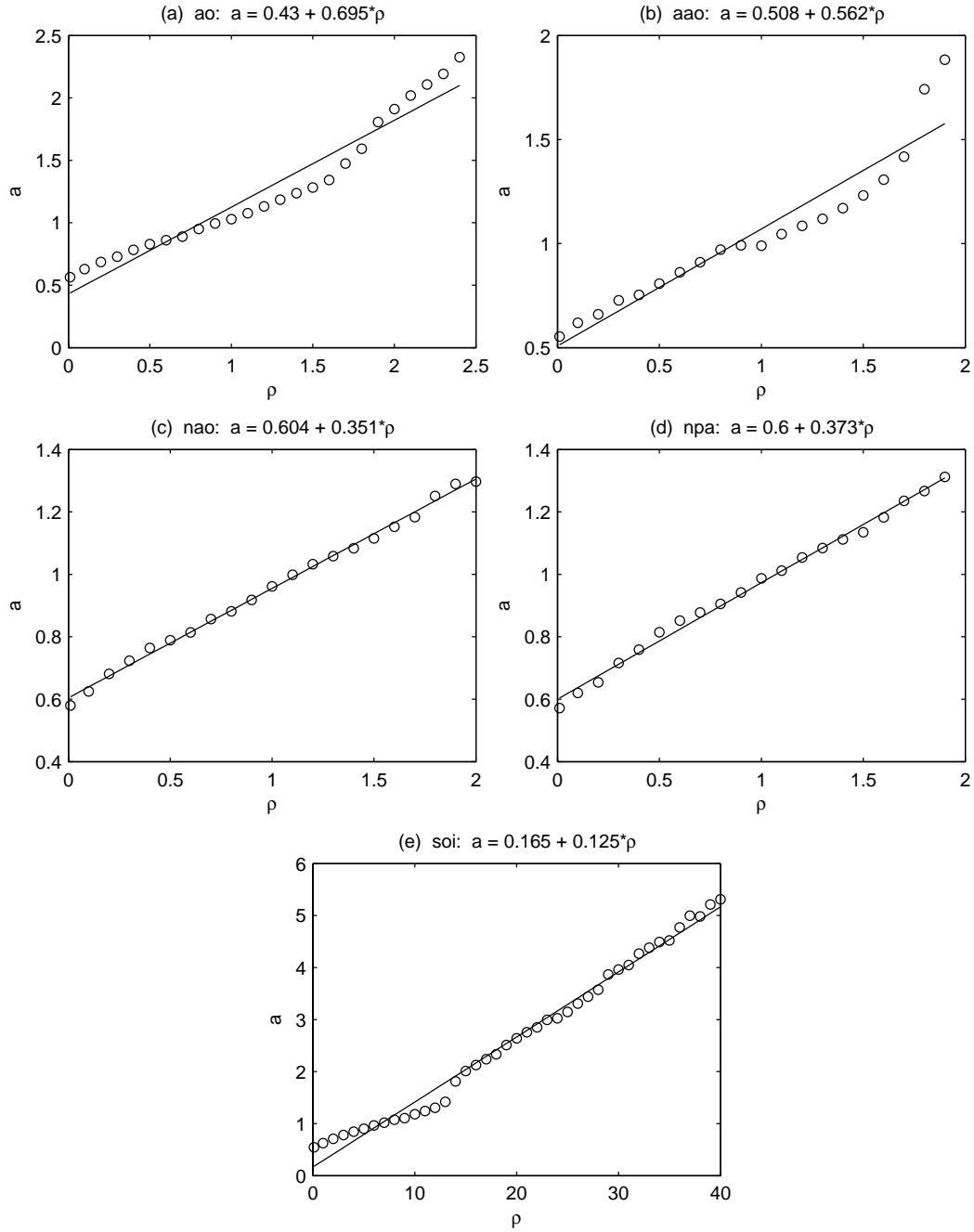
Figure 2. Histograms of the climate indices: (a) Arctic Oscillation (AO), (b) Antarctic Oscillation (AAO), (c) North Atlantic Oscillation (NAO), (d) Pacific/North American Pattern (PNA), and (e) Southern Oscillation (SO).

Figure 3. FPT density functions with particular index reduction ρ for (a) Arctic Oscillation (AO), (b) Antarctic Oscillation (AAO), (c) North Atlantic Oscillation (NAO), (d) Pacific/North American Pattern (PNA), and (e) Southern Oscillation (SO).
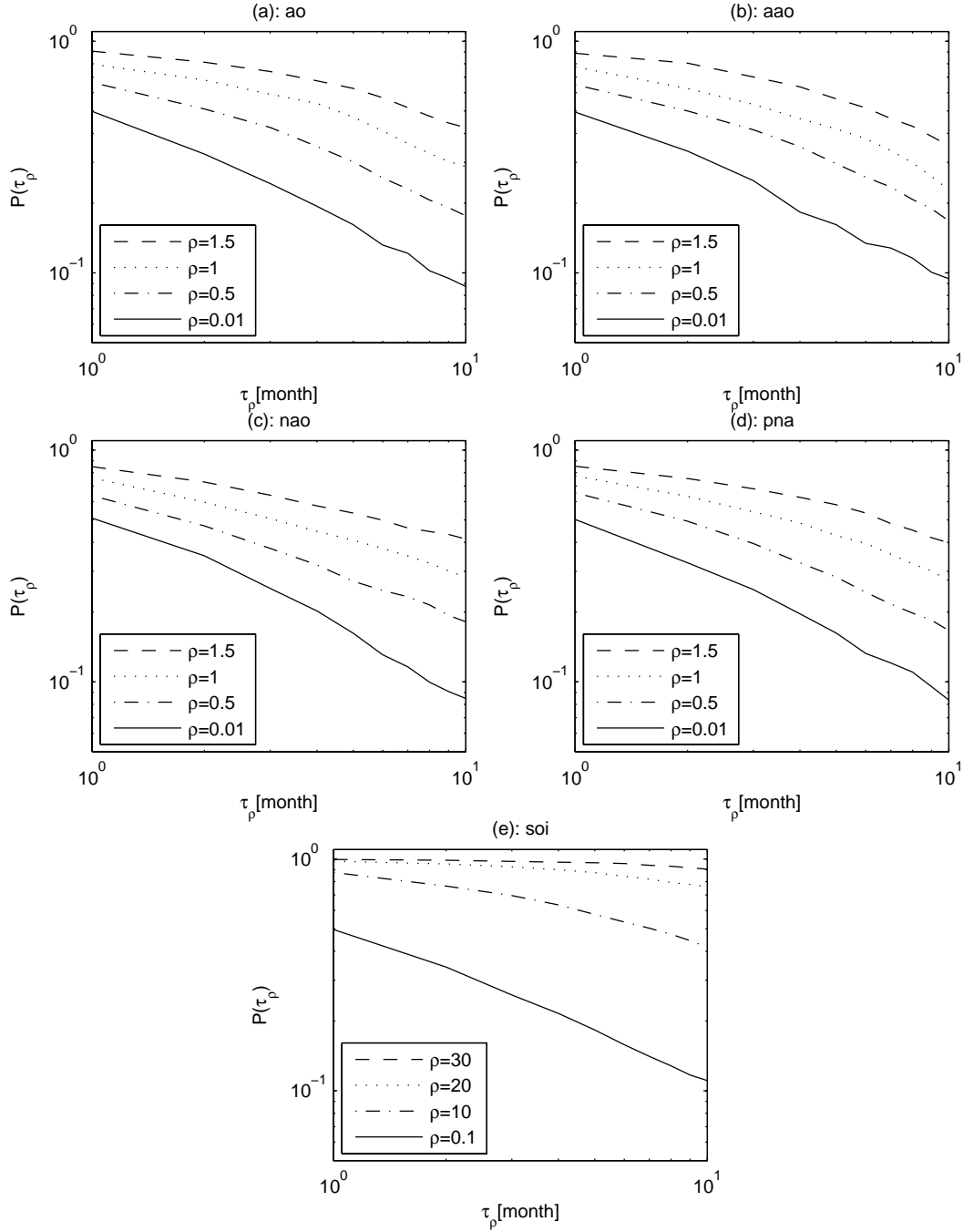
Figure 4. Linear relation ship between the parameter a in the FPT density function and the index reduction δ for (a) Arctic Oscillation (AO), (b) Antarctic Oscillation (AAO), (c) North Atlantic Oscillation (NAO), (d) Pacific/North American Pattern (PNA), and (e) Southern Oscillation (SO).

Figure 5. The empirical cumulative density functions, $P(\tau_\rho)$, for different values of the index reduction ρ for (a) Arctic Oscillation (AO), (b) Antarctic Oscillation (AAO), (c) North Atlantic Oscillation (NAO), (d) Pacific/North American Pattern (PNA), and (e) Southern Oscillation (SO). It shows the power-law features.
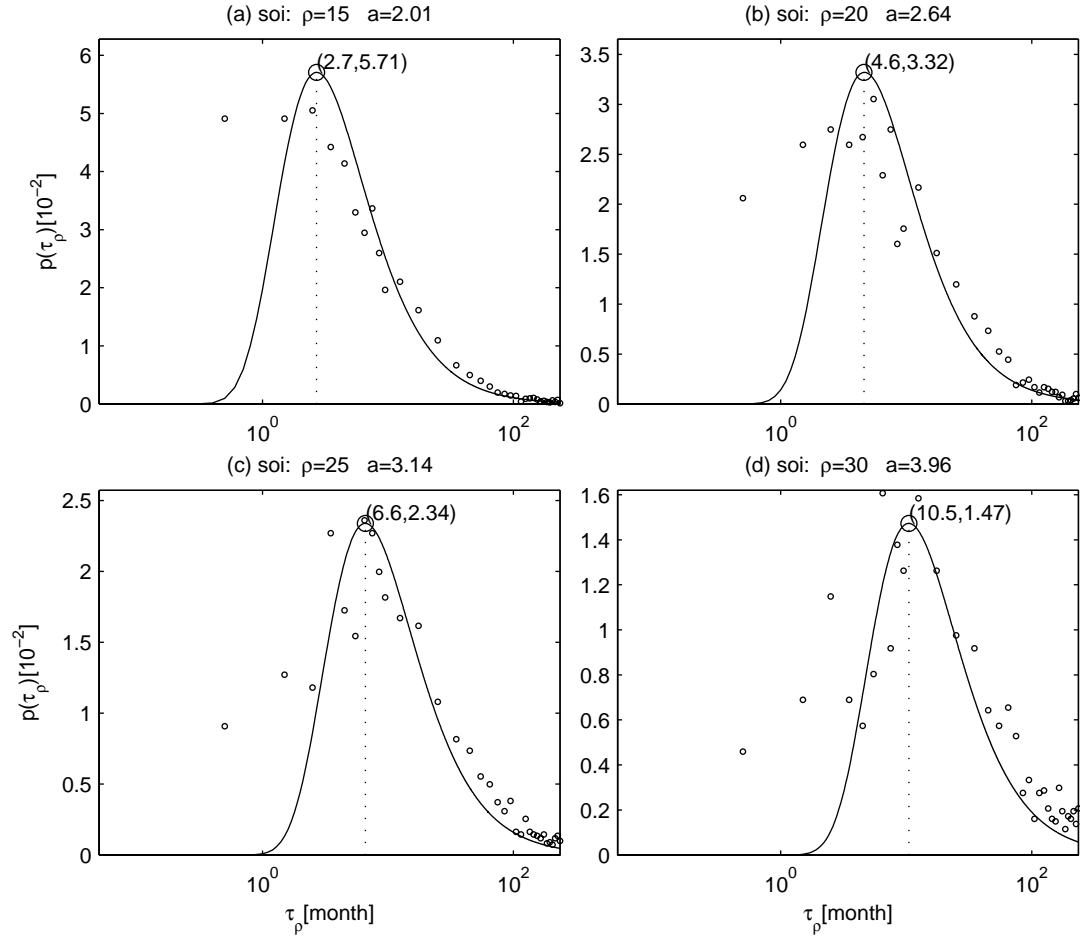
Figure 6. FPT density function of SOI with different values of ρ : (a) 15, (b) 20, (c) 25, and (d) 30. It is noted that the optimal FPT increases as ρ increases.
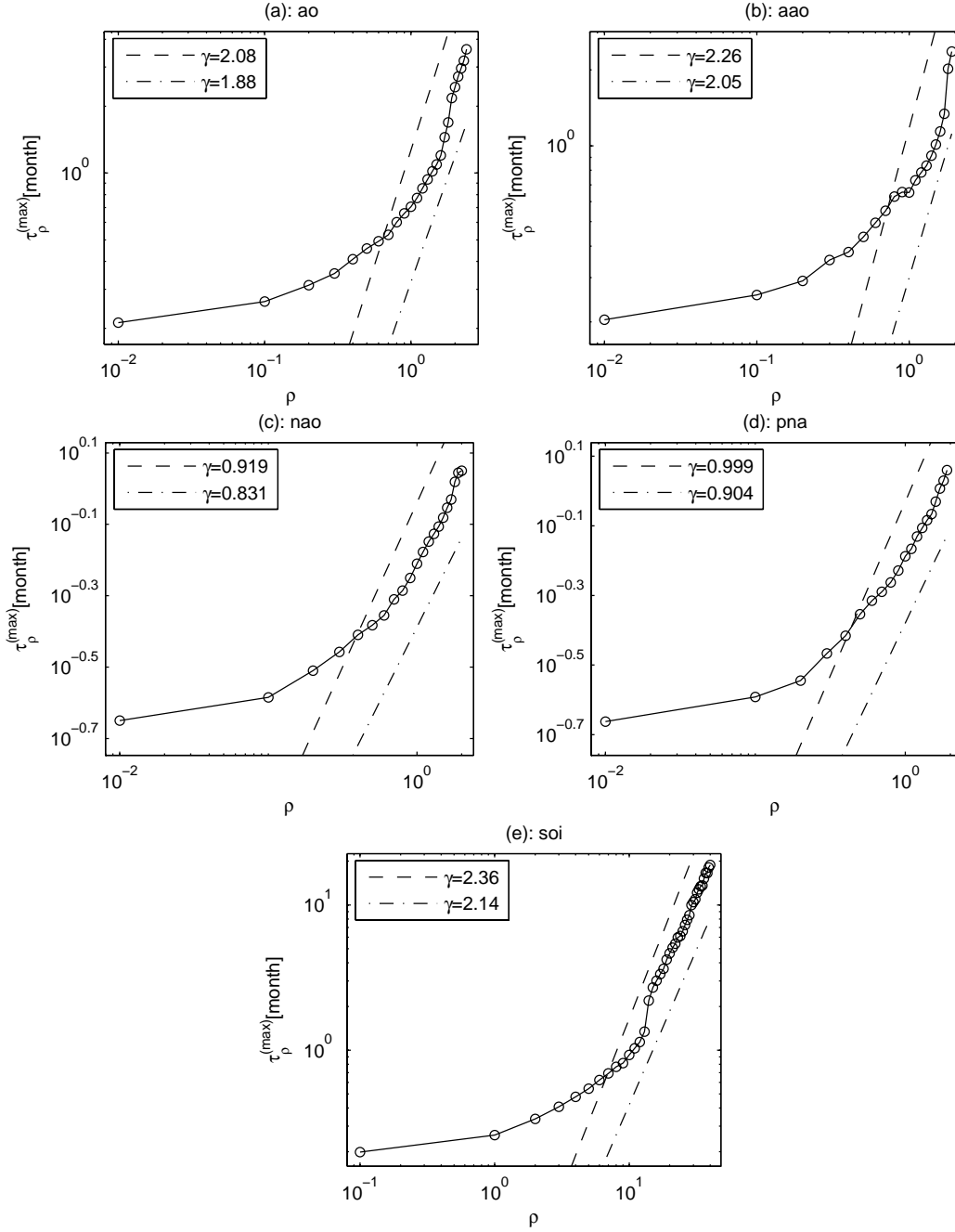
Figure 7. Dependence of the optimal FPT, $\tau_{\rho}^{(max)}$, on the index reduction ρ for (a) Arctic Oscillation (AO), (b) Antarctic Oscillation (AAO), (c) North Atlantic Oscillation (NAO), (d) Pacific/North American Pattern (PNA), and (e) Southern Oscillation (SO). Power-law exists for large ρ values.